

## ORIGINAL ARTICLE

# Perifosine and sorafenib combination induces mitochondrial cell death and antitumor effects in NOD/SCID mice with Hodgkin lymphoma cell line xenografts

SL Locatelli<sup>1,2</sup>, A Giacomini<sup>1,2</sup>, A Guidetti<sup>3,4</sup>, L Cleris<sup>5</sup>, R Mortarini<sup>5</sup>, A Anichini<sup>5,6</sup>, AM Gianni<sup>3,4,6</sup> and C Carlo-Stella<sup>1,2,6</sup>

The effects of the Akt inhibitor perifosine and the RAF/MEK/ERK inhibitor sorafenib were investigated using two CD30<sup>+</sup> Hodgkin lymphoma cell lines (L-540 and HDLM-2) and the CD30<sup>−</sup> HD-MyZ histiocytic cell line. The combined perifosine/sorafenib treatment significantly inhibited mitogen-activated protein kinase and Akt phosphorylation in two of the three cell lines. Profiling of the responsive cell lines revealed that perifosine/sorafenib decreased the amplitude of transcriptional signatures that are associated with the cell cycle, DNA replication and cell death. Tribbles homolog 3 (TRIB3) was identified as the main mediator of the *in vitro* and *in vivo* antitumor activity of perifosine/sorafenib. Combined treatment compared with single agents significantly suppressed cell growth (40–80%,  $P < 0.001$ ), induced severe mitochondrial dysfunction and necroptotic cell death (up to 70%,  $P < 0.0001$ ) in a synergistic manner. Furthermore, *in vivo* xenograft studies demonstrated a significant reduction in tumor burden ( $P < 0.0001$ ), an increased survival time (81 vs 45 days,  $P < 0.0001$ ), an increased apoptosis (2- to 2.5-fold,  $P < 0.0001$ ) and necrosis (2- to 8-fold,  $P < 0.0001$ ) in perifosine/sorafenib-treated animals compared with mice receiving single agents. These data provide a rationale for clinical trials using perifosine/sorafenib combination.

Leukemia (2013) 27, 1677–1687; doi:10.1038/leu.2013.28

**Keywords:** Akt inhibitors; Hodgkin lymphoma; tumor xenografts; sorafenib; perifosine; necroptosis

## INTRODUCTION

First-line chemo-radiotherapy leads to cure rates approaching 90 and 80% in classical Hodgkin lymphoma (cHL) patients with early- and advanced-stage disease, respectively.<sup>1,2</sup> However, 10% of patients with early-stage and 20% of those with advanced-stage disease show primary refractoriness to standard chemotherapy, and an additional 10–20% of patients ultimately relapse after achieving complete remission with standard-dose chemotherapy. High-dose chemotherapy followed by autologous and eventually allogeneic stem cell transplantation represents a second chance for a cure for refractory or relapsed patients. However, the majority of primary refractory patients and 50% of relapsed patients have low survival rates.<sup>3,4</sup> Thus, chemotherapy-refractory or -resistant patients represent an unmet medical need requiring new therapies.<sup>5</sup>

Recently, encouraging results were reported with the anti-CD30 antibody-drug conjugate Brentuximab Vedotin.<sup>6</sup> In addition, the histone deacetylase inhibitor panobinostat, the mTOR inhibitor everolimus, cytotoxic T-lymphocytes in Epstein-Barr virus-associated cases and the immunomodulatory drug lenalidomide have all been tested for their anti-cHL activity.<sup>5</sup> However, to date, phase I/II clinical studies investigating targeted agents as single molecules have shown limited antitumor activity.<sup>7–9</sup>

Although the exact molecular mechanisms leading to cHL transformation remain unclear, several signaling pathways, including the mitogen-activated protein kinase (MAPK), PI3K/AKT/mTOR, nuclear factor- $\kappa$ B, Jak/STAT, and Notch-1 pathways, are

deregulated in Reed-Sternberg cells,<sup>10–12</sup> and their simultaneous targeting might result in enhanced antitumor effects.

The alkylphospholipid perifosine is an oral Akt inhibitor that is currently in phase III clinical trials<sup>13,14</sup>, and has been shown to inhibit Akt<sup>15</sup> as well as MAPK.<sup>16</sup> Perifosine has also been shown to induce synergistic tumor cell death in combination with etoposide,<sup>17</sup> UCN-1<sup>18</sup> and histone deacetylase inhibitors.<sup>19</sup> Sorafenib (Nexavar, BAY43-9006) is a multikinase inhibitor that targets RAF kinase, vascular endothelial growth factor receptor-2, platelet-derived growth factor- $\alpha$  and - $\beta$ , and c-KIT to deliver antiproliferative, proapoptotic and antiangiogenic effects on a variety of solid tumors and hematopoietic malignancies.<sup>20,21</sup>

The aim of the present study was to investigate the preclinical rationale for the use of perifosine/sorafenib in cHL by analyzing the activity and mechanism(s) of action of these molecules both *in vitro* and *in vivo*. Our data demonstrate that perifosine/sorafenib combination induced specific gene expression profiling and signaling changes that were associated with a significant enhancement in the antitumor activities of the two-drug combination compared with single-agent treatment.

## MATERIAL AND METHODS

### Reagents

Perifosine was provided by Aeterna Zentaris (Frankfurt, Germany, EU), and sorafenib from Bayer AG (Leverkusen, Germany, EU). Z-VADfmk and Necrostatin-1 were purchased from R&D Systems (Minneapolis, MN, USA).

<sup>1</sup>Department of Oncology and Hematology, Humanitas Cancer Center, Humanitas Clinical and Research Center, Rozzano (MI), Italy; <sup>2</sup>Department of Medical Biotechnology and Translational Medicine, University of Milano, Italy; <sup>3</sup>Department of Medical Oncology, Fondazione IRCCS Istituto Nazionale dei Tumori, Milano, Italy; <sup>4</sup>Department of Medical Physiopathology and Transplants, University of Milano, Milano, Italy and <sup>5</sup>Department of Experimental Oncology and Molecular Medicine, Fondazione IRCCS Istituto Nazionale dei Tumori, Milano, Italy. Correspondence: Dr AM Gianni, Department of Medical Oncology, Fondazione IRCCS Istituto Nazionale Tumori, Via Venezian 1 20133, Milano, Italy. or Professor C Carlo-Stella, Department of Onco/Hematology, Humanitas Clinical and Research Center, Via Manzoni, 56 20089 Rozzano (Milano), Italy.

E-mail: alessandro.gianni@unimi.it or carmelo.carlostella@unimi.it

<sup>6</sup>These authors are senior co-authors.

Received 20 September 2012; revised 21 January 2013; accepted 24 January 2013; accepted article preview online 30 January 2013; advance online publication, 19 February 2013

## Cell lines

L-540,<sup>22</sup> HDLM-2<sup>23</sup> and HD-MyZ<sup>24</sup> cell lines were purchased from the German Collection of Microorganisms and Cell Cultures (DSMZ, Braunschweig, Germany, EU). Although these cell lines are bona fide considered cHL cell lines, they include two CD30<sup>+</sup> HL cell lines (L-540 and HDLM-2 cell lines) bearing a T-cell phenotype, and the CD30<sup>-</sup>/CD68<sup>+</sup> HD-MyZ histiocytic cell line.<sup>25</sup>

## Viable cell countings

Annexin-V-fluorescein isothiocyanate /propidium iodide (PI) double staining (Immunostep, Salamanca, SP, EU) supplemented with Flow-Count beads (Beckman Colter, Milan, Italy, EU) was used to detect viable cells, that is, Annexin-V<sup>-</sup>/PI<sup>-</sup>, by flow cytometry. Absolute cell counts were calculated by the following equation: viable cells (Annexin-V<sup>-</sup>/PI<sup>-</sup>) × total beads/counted beads.<sup>26</sup>

## Cell death assay

Dead cells, including Annexin-V<sup>+</sup>/PI<sup>+</sup> and Annexin-V<sup>-</sup>/PI<sup>+</sup> cells, were detected by Annexin-V/PI double staining and flow cytometry. Cells were analyzed on a (fluorescence activated cell sorter)Calibur flow cytometry system (BD, San Jose, CA, USA) equipped with a Macintosh PowerMac G4 personal computer (Apple Computer Inc. Cupertino, CA, USA) using BD CellQuest software version 3.3 (BD). Data were analyzed using FlowJo 8.7.1 (Tree Star, Inc. Ashland, OR, USA) software.

## Cell cycle analysis

Cells were cultured under appropriate conditions for 48 h, fixed in 70% ethanol and then stained with 2.5 µg/ml PI (Calbiochem, Darmstadt, Germany). Cell cycle was measured using a (fluorescence activated cell sorter)Calibur flow cytometry system (BD) and analyzed using the FlowJo software (Tree Star, Inc. Ashland, OR, USA).

## Measurement of $\Delta\Psi_m$

Mitochondrial membrane depolarization was determined using the fluorescent probe tetramethylrhodamine ethyl ester (Invitrogen, Milan, Italy, EU), and analyzed by flow cytometry.<sup>27</sup>

## Measurement of reactive oxygen species (ROS)

Oxidative damage was assessed by staining with the membrane permeable dye, dihydroethidium (Invitrogen), which is oxidized to ethidium in the presence of ROS, intercalates within double-stranded DNA, and then fluoresces maximally at 600 nm.<sup>27</sup> Cells ( $0.4 \times 10^6$ /ml) were stained at a final concentration of 5 µM HE for 30 min at 37 °C.

## Subcellular fractions and western blot analysis

Immunoblot analysis was performed using antibodies to apoptosis-inducing factor, Cytochrome c, Mcl-1, caspase-8, pMEK, pERK1/2, pAKT(T308), pS6 (Cell Signaling, Danvers, MA, USA), caspase-3 (Santa Cruz, San Diego, CA, USA), caspase-9, poly(ADP-ribose)polymerase (BD), and tribbles homology 3 (TRIB3) (Sigma-Aldrich, Milan, Italy, EU). Mitochondrial and cytosolic fractions were obtained using a Mitochondria/Cytosol Fractionation Kit (Biovision, Milpitas, CA, USA). Densitometry was performed using ImageJ software (<http://rsb.info.nih.gov/ij/>).

## Phospho-kinase proteome profiler array

The human phospho-kinase array proteome profiler (R&D) was used to assess the basal phosphorylation levels of the Akt pathway (for details, see Supplementary Material).

## Genome-wide expression profiling

RNA integrity and purity of treated cells was assessed using Bioanalyzer (Agilent Technologies, Milano, Italy, EU). Hybridization was performed on Illumina Bead Chip HumanHT-12\_v3 Microarrays (Illumina, San Diego, CA, USA). The expression profiles was deposited in NCBI's Gene Expression Omnibus GSE31060. Data were analyzed with BeadStudio Illumina software and Ingenuity Pathway Analysis ([www.ingenuity.com](http://www.ingenuity.com)) (for details, see Supplementary Material).

## Quantitative reverse transcription-PCR

*TRIB3*, *DDIT4*, *CCNE1*, *CDC25A*, and *PLEKHF1* genes, were analyzed with TaqMan isoform-specific probe (Applied Biosystems, Foster City, CA, USA), and referred to  $\beta$ 2-microglobulin as housekeeping gene, using the  $\Delta\Delta C_t$  method (for details, see Supplementary Material).

## siRNA gene silencing

L-540 cells were transfected with 100 nM of either Hs-TRIB3 FlexiTube small interfering RNA (siRNA) or the negative-control siRNA premix reagent (Qiagen, Milano, Italy), according to the instructions of the manufacturer. The cells ( $0.4 \times 10^6$ /ml) were plated and transfected with the given siRNAs. After 24 h, the cells were treated with perifosine and sorafenib as indicated. Gene silencing effects were evaluated by western blot and viable cell counting, as described above, after 48 and 72 h of drug treatments, respectively.

## Activity of perifosine/sorafenib in tumor-bearing nonobese diabetic/severe combined immunodeficient mice

Six- to eight-weeks-old nonobese diabetic/severe combined immunodeficient mice with a body weight of 20–25 g were purchased from Charles

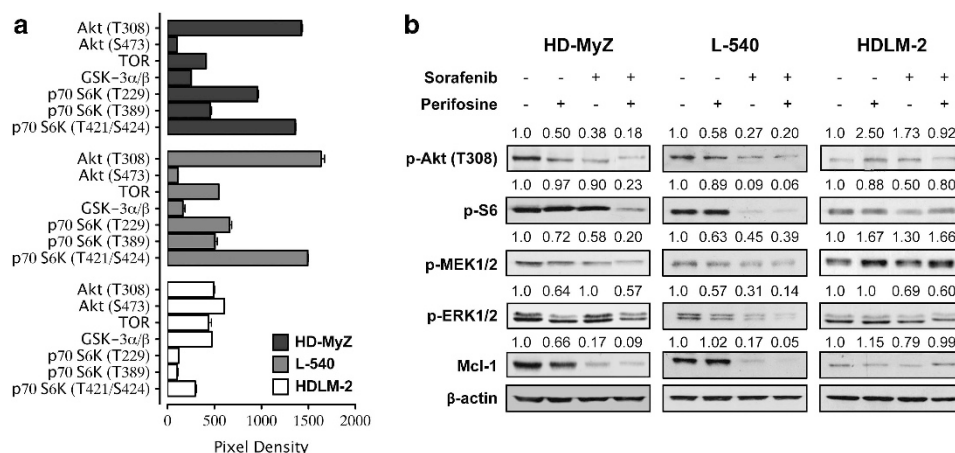


**Figure 1.** Perifosine/sorafenib treatment affects the Akt and MAPK pathways. **(a)** Baseline phosphorylation levels of Akt, and its downstream targets in HD-MyZ, L-540 and HDLM-2 cells. The chemiluminescence signal intensity of individual spots was analyzed using the open source imaging software ImageJ. The assays were conducted in duplicate. The data shown are from one of two independent experiments. **(b)** Immunoblots of extracts from HD-MyZ, L-540 and HDLM-2 cells treated with perifosine (5 µM) and/or sorafenib (5 µM) for 16 h. Relative protein levels referred to vehicle control-treated cells were obtained by dividing total values of each protein by the corresponding actin value. Experiments were repeated twice with similar results. Representative blots are shown.

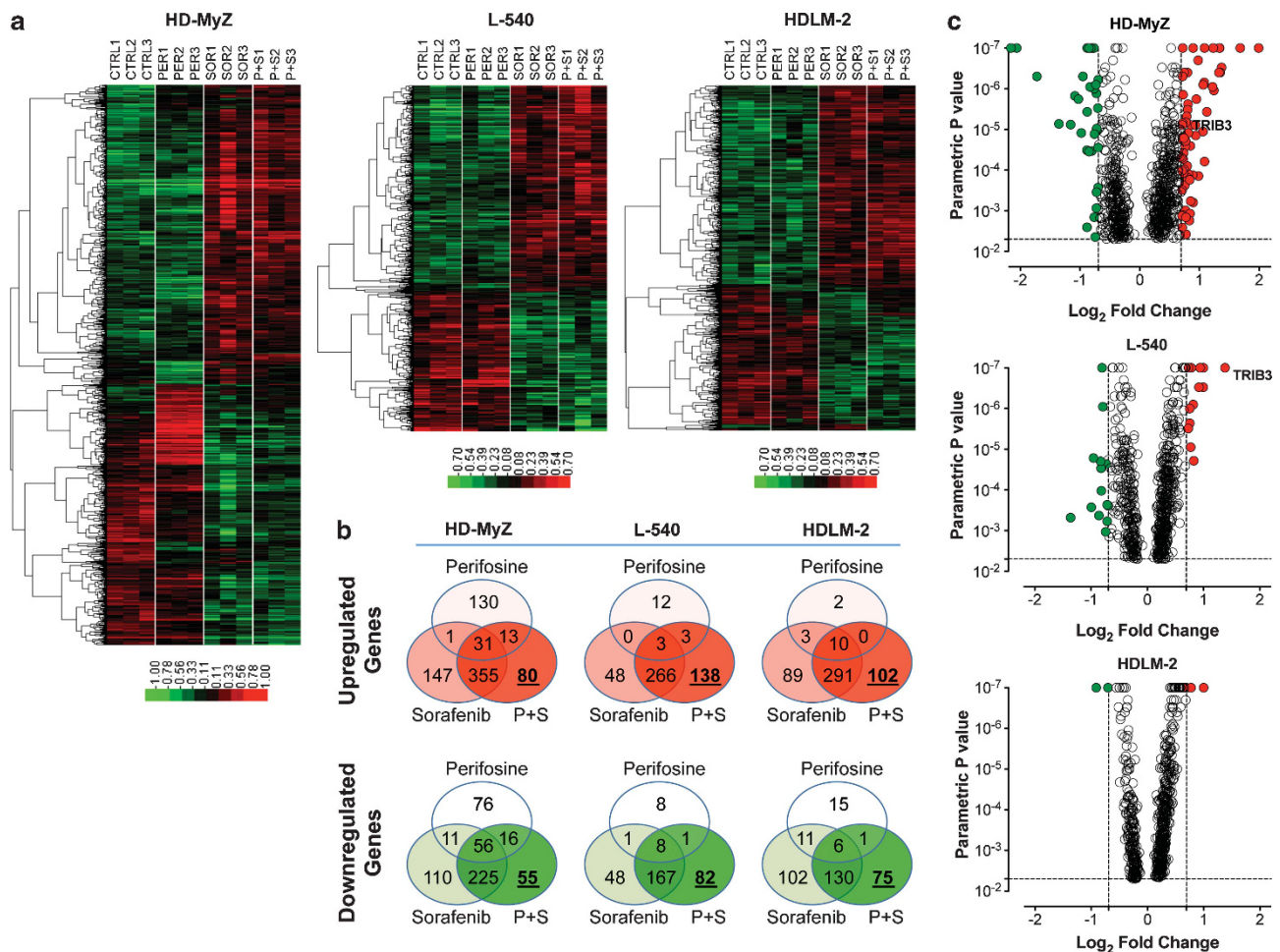


**Figure 2.** Modulation of gene expression by perifosine, sorafenib or both. **(a)** One-way hierarchical clustering of genes (HD-MyZ  $n = 1242$ , L-540  $n = 778$  and HDLM-2  $n = 829$ ) showed significant modulation (at  $P = 0.005$  in the univariate F-test) by perifosine ( $10 \mu\text{M}$ ) and/or sorafenib ( $5 \mu\text{M}$ ) treatment, after 24 h. Gene-wise median-centered normalized intensities (in Log space) of untreated cells (CTRL1–3) and of cells treated with perifosine (PER1–3), sorafenib (SOR1–3) or the perifosine/sorafenib combination (P + S1–3) are shown. The heat map was clustered using centered correlation as the distance metric and complete linkage clustering. **(b)** Venn diagram analysis of significantly modulated genes by perifosine, sorafenib or their combination in the three cHL lines. Numbers indicated in bold and underlined highlight genes that were significantly modulated only by the perifosine/sorafenib combination. **(c)** Volcano plots of all genes that were significantly modulated by the perifosine/sorafenib combination, demonstrating the extent of modulation (as Log<sub>2</sub> fold change) vs the  $P$ -value obtained from the univariate F-test. Vertical dotted bars:  $\pm 1.5$ -fold changes. Horizontal dotted line identifies the  $P = 0.005$  nominal significance value of the univariate F-test.

River (Milano, Italy, EU) and xenografted with HD-MyZ, L-540, or HDLM-2 cells. Animal experiments were performed according to Italian laws (D.L. 116/92 and following additions), and were approved by the institutional Ethical Committee for Animal Experimentation. For survival experiments, mice were inoculated intravenously with HD-MyZ cells ( $1.8 \times 10^6$  cells/mouse), and 3 days after tumor injection were randomized to receive perifosine (7.5 mg/kg/mouse, per os, 5 days/weeks, for 5 weeks) and/or sorafenib (60 mg/kg/mouse, intraperitoneally (IP), 5 days/weeks, for 5 weeks) or control vehicle. Activity of drug combination was also analyzed in subcutaneous xenograft models. HD-MyZ ( $5 \times 10^6$  cells/mouse), L-540 and HDLM-2 ( $25 \times 10^6$  cells/mouse) cells were inoculated into the left flank of each mouse. When tumor volume reached  $\sim 100$  mg in weight, mice were randomly assigned to receive either a short- or long-term treatment. The short-term treatment consisted of perifosine (30 mg/kg/mouse for 5 days) and/or sorafenib (90 mg/kg/mouse for 5 days, IP) and was used to assess tumor necrosis and apoptosis. For the long-term treatment, 7 and 11 days following L-540 and HDLM-2 cell inoculation, respectively, mice were treated with perifosine (15 mg/kg/mouse, 5 days/week for 3 weeks) and/or sorafenib (30 mg/kg/mouse for 5 days/week for 3 weeks). Tumor weights were calculated using the following formula:  $(a \times b^2)/2$ , where  $a$  and  $b$  represent the longest and shortest diameters, respectively. Tumor growth inhibition was defined as  $(1 - (T/C) \times 100)$ , where  $T$  and  $C$  represent the mean tumor weight in the treated and

untreated control groups, respectively. Each experiment was performed on at least two separate occasions, using five mice per treatment group.

#### Histological analysis of tumor nodules

Sections from formalin-fixed, paraffin-embedded tumor nodules were stained with hematoxylin and eosin. Apoptosis and tumor necrosis were detected using TdT-mediated dUTP nick end-labeling (TUNEL) staining (Roche, Milano, Italy, EU).

#### Immunofluorescence and confocal microscopy

Epitope retrieval on formalin-fixed, paraffin-embedded nodules was performed with 10 mM Sodium citrate buffer. Sections were initially incubated with rabbit anti-human DDIT4 (1:50) and anti-TRIB3 (1:100) (Sigma-Aldrich) antibodies and subsequently with the appropriate Alexa Fluor 568-conjugated secondary antibody (Invitrogen). Finally, sections were incubated with TO-PRO-3 nuclear dye (1:10 000) (Invitrogen), and examined under an epifluorescent microscope equipped with a laser confocal system (MRC-1024, Bio-Rad Laboratories, Milan, Italy). Image processing was carried out using LaserSharp computer software (Bio-Rad Laboratories).<sup>28</sup>

#### Analysis of stained sections

Image analysis was carried out using the open source ImageJ software.<sup>28</sup>

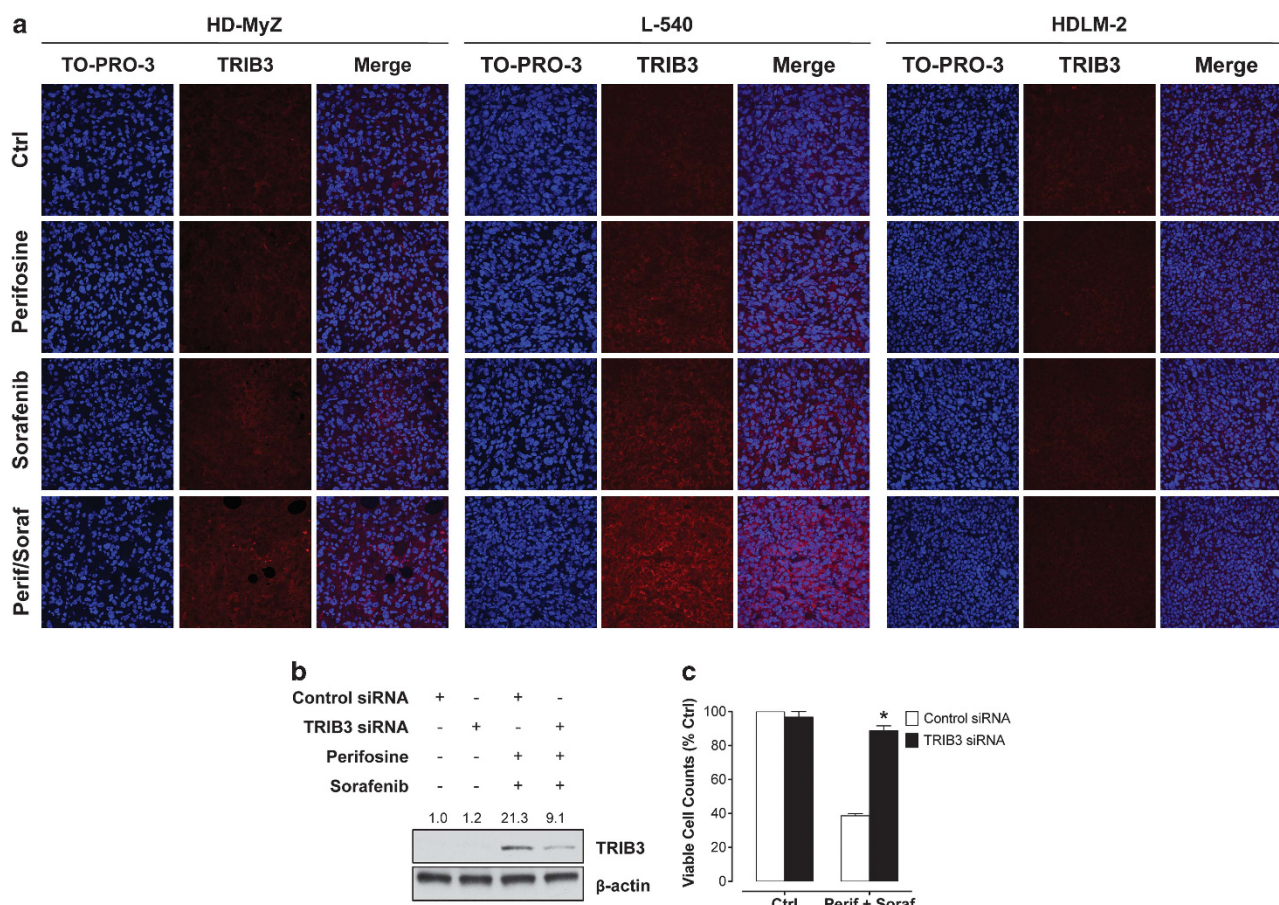


**Figure 3.** Role of TRIB3 induction in perifosine/sorafenib-induced cell death. **(a)** Nonobese diabetic/severe combined immunodeficient (NOD/SCID) mice bearing HD-MyZ, L-540 and HDLM-2 tumor nodules were treated with perifosine (30 mg/kg/5die, per os (PO)) or sorafenib (90 mg/kg/5die, IP) (either alone or in combination) or vehicle control. Representative confocal images of tumors from untreated and treated animals that were processed by double immunofluorescence staining are shown. Cell nuclei (blue) were detected using TO-PRO-3. TRIB3 expression (red) was detected using the anti-TRIB3 antibody and an Alexa Fluor 568-conjugated secondary antibody. Objective lens, original magnification: 1.0 numerical aperture (NA) oil objective,  $\times 40$ . **(b)** and **(c)** L-540 cells were transfected with TRIB3 siRNA (100 nM) and control siRNA (100 nM) overnight. After transfection, the cells were treated with perifosine and/or sorafenib for 48–72 h. **(b)** After 48 h, the efficiency of TRIB3 siRNA inhibition was analyzed by western blotting using a TRIB3-specific antibody. Each lane was subjected to densitometric analysis as described in the Material and methods section. Representative blots are shown. The experiments were repeated twice with similar results. **(c)** Viable cell counts after 72 h were obtained as described in the Material and methods. Mean ( $\pm$  s.e.m.) values refer to three independent experiments. \* $P < 0.001$  in comparison with control siRNA.

### Statistical analysis

Statistical analysis was performed with the statistical package Prism 6 (GraphPad Software, San Diego, CA, USA) using a Macintosh Pro personal computer (Apple Computer Inc.). To test the probability of significant differences between untreated and treated samples, a two-way analysis of variance was used, and individual group comparisons were evaluated using a Bonferroni post-test. Survival curves were created using the product limit method of Kaplan-Meier, and survival differences were compared using the logrank test. TUNEL staining data were statistically analyzed using one-way analysis of variance, and individual group comparisons were evaluated using a Bonferroni post-test. Differences were considered significant at the level of  $P \leq 0.05$ . Interaction between perifosine and sorafenib was analyzed using the median dose analysis of Chou and Talalay.<sup>29</sup> Normalized isobolograms and combination indexes for non constant drug ratios were obtained by the CalcuSyn software (Bio-Soft Inc. Cambridge, MA, USA). Combination index values  $< 1.0$  indicate a synergistic interaction.

## RESULTS

Inhibition of MAPK and Akt pathways is strongly enhanced by the perifosine/sorafenib combination treatment

HD-MyZ, L-540 and HDLM-2 cell lines were initially characterized for their baseline levels of the phosphorylation of relevant targets

in the AKT pathway (Figure 1a). Interestingly, HDLM-2 cells showed low basal levels of phospho-Akt and p-p70S6K compared with HD-MyZ and L-540 cells, which highlights a potential difference between these lines in terms of their response to inhibitors of this pathway.<sup>30</sup> In fact, treatment of cells with single agents resulted in a partial inhibition of target phosphorylation in HD-MyZ and L-540 cells, but not in HDLM-2 cells (Figure 1b). In contrast, the combined treatment resulted in an almost complete inhibition of target phosphorylation in HD-MyZ and L-540 cell lines: the levels of phospho-Akt were reduced by 80% in both cell lines, those of p-ERK were reduced by 43 and 86% in the HD-MyZ and L-540 cell lines, respectively, and the expression of Mcl-1 was almost completely abrogated in both cell lines. Once again, no effect could be detected in the HDLM-2 cell line (Figure 1b).

### Modulation of gene expression by the perifosine/sorafenib combination

To gain further insight into the effects of perifosine, sorafenib and their combination, we performed a genome-wide microarray analysis of HD-MyZ, L-540 and HDLM-2 cell lines that had been treated for 24 h with these inhibitors. Heat maps (Figure 2a) and

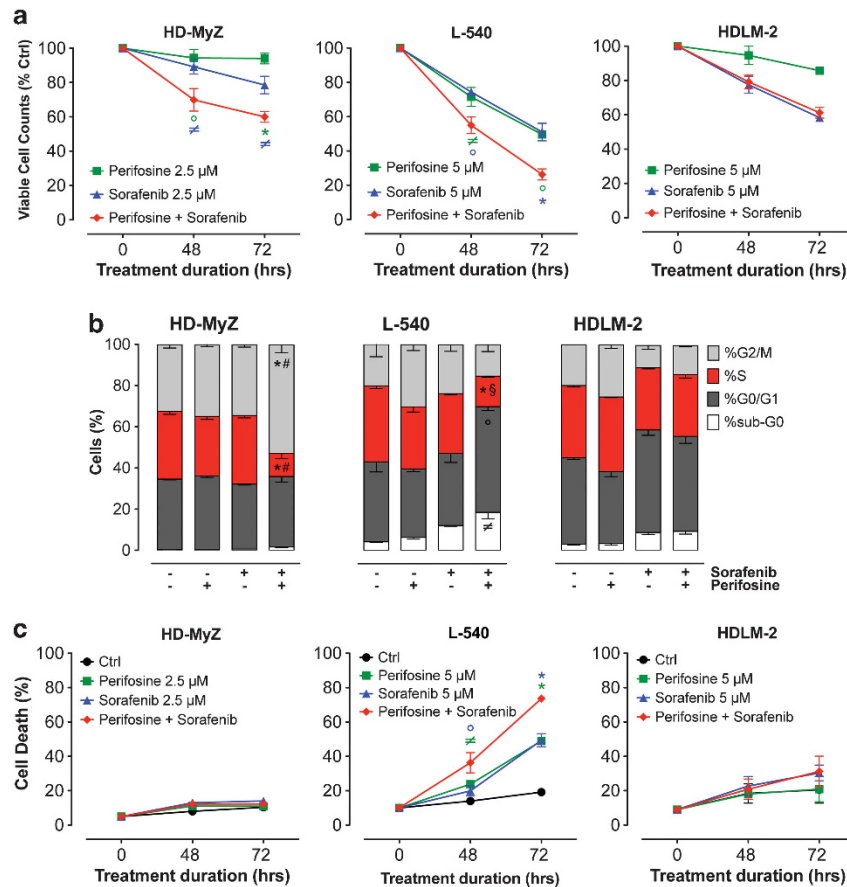


**Figure 4.** Coadministration of perifosine and sorafenib results in a striking increase in cell death, cell cycle arrest and diminished viability. (a) HD-MyZ, L-540 and HDLM-2 cells were exposed to perifosine (green) and sorafenib (blue) either alone or in combination (red) for 48 and 72 h, after which point viable cell counts were obtained as described in the Material and methods section. Mean ( $\pm$  s.e.m.) values refer to three independent experiments.  $^*P < 0.0001$ ,  $^{\circ}P < 0.001$ , and  $^{\#}P < 0.01$  in comparison with single treatments. (b) Cell cycle analysis of the combined treatment of perifosine (2.5  $\mu$ M) and sorafenib (2.5  $\mu$ M) on HD-MyZ cells, and treatment with perifosine (5  $\mu$ M) and sorafenib (5  $\mu$ M) on L-540 and HDLM-2 cells after 48 h. Flow cytometry was performed to define the cell cycle distribution of treated cells in comparison with untreated controls. Mean ( $\pm$  s.e.m.) values refer to three independent experiments.  $^*P < 0.0001$  and  $^{\#}P < 0.05$  in comparison with the control,  $^{\circ}P < 0.01$  and  $^{\#}P < 0.05$  in comparison with single treatments. (c) HD-MyZ, L-540 and HDLM-2 cells were exposed to perifosine (green) and sorafenib (blue) either alone or in combination (red) for 48 and 72 h, after which point the percentage of dead cells was obtained as described in the Material and methods. Mean ( $\pm$  s.e.m.) values refer to three independent experiments.  $^*P < 0.0001$ ,  $^{\circ}P < 0.001$ , and  $^{\#}P < 0.01$  in comparison with single treatments.

Venn diagram analysis (Figure 2b) of significantly modulated genes indicated a dominant role for sorafenib in changing gene expression levels, with less impact by perifosine, in all three cell lines. In fact, as shown by the Venn diagrams, (Figure 2b) sorafenib modulated a larger number of genes than perifosine, and most of the genes that were modulated by the 'sorafenib only' treatment remained modulated even in the perifosine/sorafenib combination. However, in all three cell lines, the Venn diagram analysis identified genes that were also significantly modulated by the perifosine/sorafenib combination (Figure 2b lower right circles, bold underlined numbers in each Venn diagram and Supplementary Table 1a–c for the identity and fold change values of all significantly modulated genes). Volcano plots of the latter subsets of genes indicated that only a small group of these genes underwent a strong modulation (that is, a fold change  $> 1.5$ ) following perifosine/sorafenib treatment (Figure 2c). Ingenuity pathway analysis of the genes that were significantly modulated by the perifosine/sorafenib combination (Supplementary Table 2a–c) was also performed. In HD-MyZ cell line, the most up and downregulated genes (indicated in bold red or green in Supplementary Table 2a, respectively) were part of interacting networks, and/or had functions related to cellular movement, cell cycle and cell death, DNA replication, cellular growth and

proliferation. In this cell line, genes inhibited by the perifosine/sorafenib combination were part of canonical pathways regulating cell cycle progression (Supplementary Table 2a). In the same cell line, we then searched for genes that showed enhanced modulation following perifosine/sorafenib combined treatment compared with single-agent treatment. Some of these genes, including *DDIT4/REDD1*, a negative regulator of mTOR pathway (Supplementary Figure 1a),<sup>31</sup> were validated by reverse transcription-PCR (Supplementary Figure 1b) and confocal microscopy on tumor nodules treated with the inhibitors (Supplementary Figure 1c). Interestingly, only one of these genes, *TRIB3*, a 45-KDa pseudokinase that binds to and inhibit both Akt<sup>32</sup> and MAPK Kinases,<sup>33</sup> was significantly modulated by the combined treatment in the two most responsive cell lines (HD-MyZ and L-540, Figure 2c), which suggested a potential role for this gene in the antitumor effect of the combined treatment.

Perifosine/sorafenib-mediated antitumor effect involves *TRIB3* upregulation

Whereas, baseline levels of *TRIB3* expression were negligible in all cell lines, the combined perifosine/sorafenib treatment resulted in a significant enhancement of *TRIB3* expression in HD-MyZ and

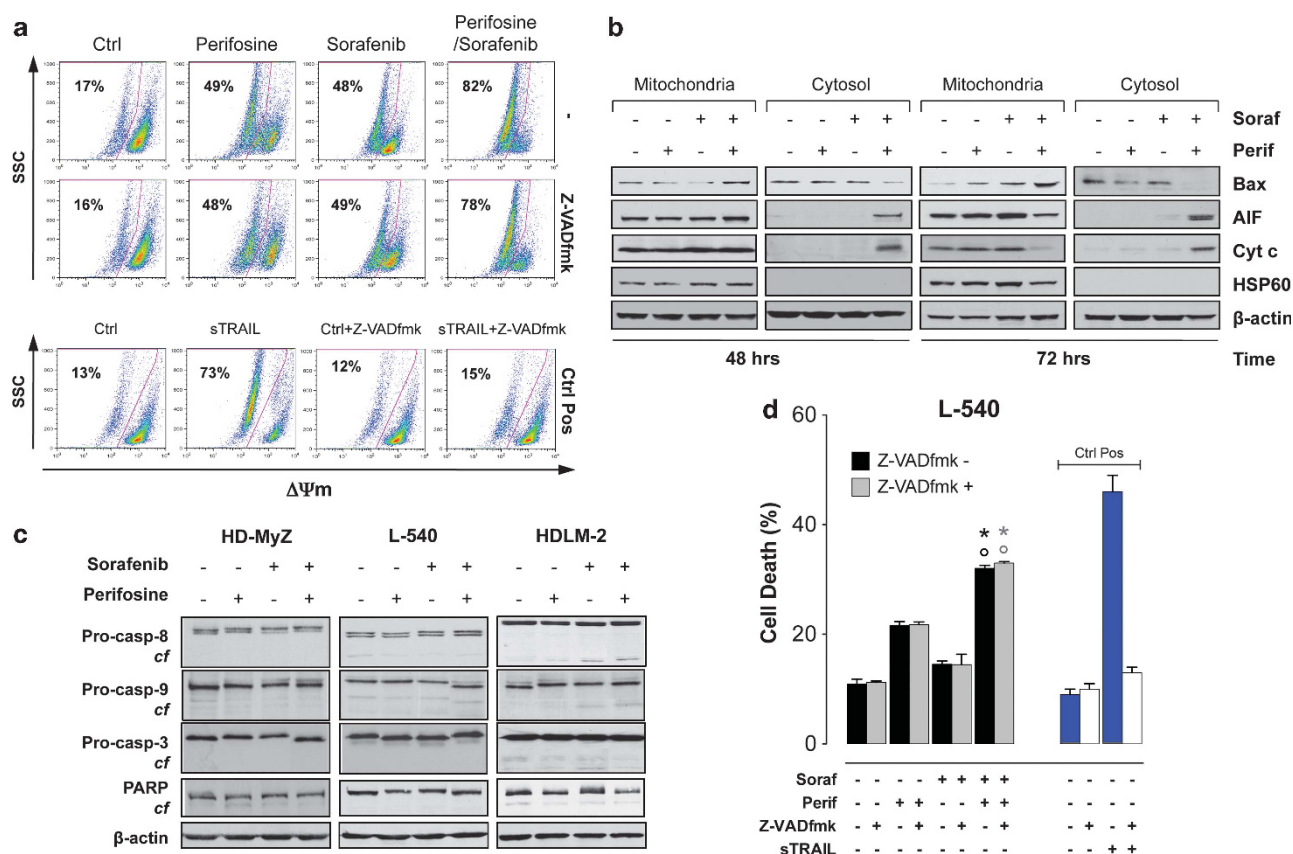


**Figure 5.** Exposure to the perifosine/sorafenib combination results in a marked increase in mitochondrial injury and caspase-independent cell death. **(a)** L-540 cells were treated with perifosine (5  $\mu$ M) and/or sorafenib (5  $\mu$ M) in the absence or presence of Z-VADfmk (50  $\mu$ M). Treatment with the caspase inhibitor Z-VADfmk was initiated 1 h before the addition of perifosine and sorafenib. After 72 h, loss of mitochondrial potential ( $\Delta\Psi_m$ ) was measured using tetramethylrhodamine ethyl ester staining and flow cytometry. Shown are representative dot plots of mitochondrial membrane depolarization. KMS-11 cell line exposed to sTRAIL 10 ng/ml was used as positive control for mitochondrial depolarization inhibition after Z-VADfmk treatment. **(b)** L-540 cells were exposed to 5  $\mu$ M sorafenib and 5  $\mu$ M perifosine alone or in combination for 48–72 h, after which point the mitochondrial and cytosolic fractions were obtained and subjected to western blot analysis to monitor conformational changes in Bax, release of cytochrome c and apoptosis-inducing factor (AIF). The purity of the mitochondrial and cytosolic fractions was determined by western blot analysis using an anti-HSP60 antibody. **(c)** HD-MyZ, L-540 and HDLM-2 cells were treated with perifosine (5  $\mu$ M), sorafenib (5  $\mu$ M) or both for 48 h. Whole-cell lysates were obtained, and western blot analysis was used to monitor caspase cleavage/activation and poly(ADP-ribose)polymerase degradation. Cf indicates cleaved fragments. **(d)** L-540 cells were pretreated with 50  $\mu$ M Z-VADfmk for 1 h and then treated with 5  $\mu$ M perifosine  $\pm$  5  $\mu$ M sorafenib for 48 h. Following the treatments, cell death was assayed by flow cytometry using Annexin V/PI double staining. KMS-11 cell line exposed to sTRAIL 10 ng/ml was used as positive control for mitochondrial depolarization inhibition after Z-VADfmk treatment. \* $P$  < 0.0001 in comparison with sorafenib alone, ° $P$  < 0.001 in comparison with perifosine alone. Mean ( $\pm$  s.e.m.) values refer to three independent experiments.

L-540, but not HDLM-2 tumor nodules (Figure 3a). To define whether the antitumor activity of the combined perifosine/sorafenib treatment required the upregulation of TRIB3, we silenced the expression of TRIB3 using TRIB3 siRNA and then examined cell sensitivity to the perifosine/sorafenib combined treatment. By western blotting, we detected substantially reduced levels of TRIB3 (43% reduction) in L-540 cells transfected with TRIB3 siRNA compared with control siRNA-transfected cells (Figure 3b), which led to a 50% increase in cell viability after perifosine/sorafenib combined treatment (Figure 3c). These results indicate that TRIB3 upregulation is involved in the antitumor effect of perifosine/sorafenib.

#### Perifosine/sorafenib treatment reduces cell proliferation and triggers caspase-independent cell death

To better define the effects of simultaneous Akt and ERK inhibition at the cellular level, we assessed cell proliferation and cell death in cell lines that were treated with the perifosine/sorafenib combination. A 72 h exposure to the perifosine/sorafenib combination

significantly reduced the absolute numbers of viable cells only in HD-MyZ and L-540 cells (by 40 and 74%, respectively), but not in the HDLM-2 cell line (Figure 4a), compared with the exposure to single agents. Cell cycle analysis indicated that exposure to the perifosine/sorafenib combination significantly increased the percentages of cells in G2/M phase (HD-MyZ cell line) or induced G0/G1 cell cycle arrest (L-540 cell line), although no significant cell cycle changes could be detected in the HDLM-2 cell line (Figure 4b). Upon exposure to the perifosine/sorafenib combination, the L-540 cell line (but not the HD-MyZ and HDLM-2 cell lines) showed a significant increase in cell death compared with the exposure to single agents (control:  $19 \pm 3\%$ , perifosine:  $49 \pm 3\%$ , sorafenib:  $49 \pm 8\%$ , combination  $74 \pm 4\%$ ,  $P$  < 0.0001) (Figure 4c). Median dose-effect analysis of cell death following exposure of L-540 to perifosine and sorafenib for 48 h in a range of pharmacologically achievable concentrations yielded combination indices well below 0.8, indicating synergistic interactions (Supplementary Figure 2a and b).

The mechanism of perifosine/sorafenib-induced cell death was then investigated in detail in L-540 cells. The combination of these

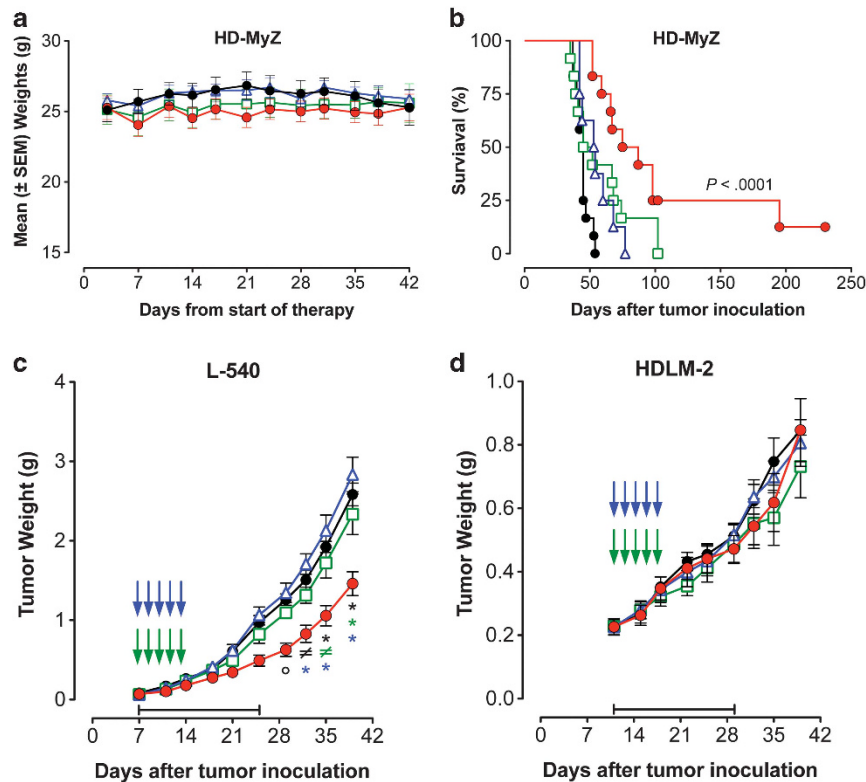


**Figure 6.** Perifosine in combination with sorafenib produces robust efficacy against tumor xenografts in NOD/SCID mice. **(a and b)** HD-MyZ cells ( $1.8 \times 10^6$  cells/mouse) were intravenously injected into NOD/SCID mice. Mice received vehicle control (black), perifosine (7.5 mg/kg/mouse, 5 days/weeks, for 5 weeks, PO, green), sorafenib (60 mg/kg/mouse, 5 days/weeks, for 5 weeks, IP, blue) or the combined treatment (red). Treatment began at day 3 post-tumor inoculation. Each treatment group contained 10 mice. **(a)** Mean weight ( $\pm$  s.e.m.) values were assessed. **(b)** Kaplan-Meier estimates of the overall survival of NOD/SCID mice xenografted with the HD-MyZ cell line. Survival was measured from the day of xenografting.  $*P < 0.0001$  in comparison with controls. Perifosine plus sorafenib-induced *in vivo* cHL tumor growth inhibition. **(c and d)** Control vehicle (black), perifosine (15 mg/kg, 5 days/weeks, for 3 weeks, PO, green), sorafenib (30 mg/kg, 5 days/weeks, for 3 weeks, IP, blue) and the combined treatment (red). Each experiment was performed on at least two separate occasions, using five mice per treatment group. Green arrows indicate perifosine treatment administration, and blue arrows indicate sorafenib treatment administration. For each cell line, the treatment duration is indicated by horizontal capped black lines (days 7–25 and days 11–29 for L-540 and HDLM-2 xenografts, respectively). Mean ( $\pm$  s.e.m.) tumor weight data are shown.  $*P < 0.0001$ ;  $^{\#}P < 0.001$ ;  $^{\circ}P < 0.01$ .

two inhibitors led to a marked mitochondrial depolarization (up to 80%), which was observed even in the presence of the pan-caspase inhibitor Z-VADfmk (Figure 5a). Treatment with perifosine or sorafenib resulted in the mitochondrial translocation of Bax, and this effect was strongly enhanced by the combined treatment (Figure 5b). Moreover, the association of the two inhibitors led to a marked increase of apoptosis-inducing factor and cytochrome c release in the cytosol (Figure 5b). Interestingly, the two inhibitors, used either alone or in combination, failed to induce either caspase activation (caspase 8, 9 or 3) or poly(ADP-ribose)polymerase cleavage in L-540 cells (Figure 5c). Furthermore, Z-VADfmk did not inhibit perifosine/sorafenib-induced cell death (Figure 5d), indicating a nonapoptotic mechanism of cell death.

Therefore, we investigated whether the programmed necrosis, necroptosis, was involved in perifosine/sorafenib-induced cell death by performing blocking experiments using the RIP1 kinase inhibitor Necrostatin-1,<sup>34</sup> a powerful tool allowing to detect programmed necrosis.<sup>35</sup> When L-540 cells were treated with perifosine/sorafenib in the presence of Necrostatin-1, cell death was completely prevented (Supplementary Figure 3a). Additionally, Necrostatin-1 almost completely prevented perifosine/sorafenib-induced production of ROS, as well as TRIB3 induction (Supplementary Figure 3b and c). In order to elucidate the role of TRIB3 in ROS generation, we also assessed ROS generation after transfecting perifosine/sorafenib-treated L-540 cells with a TRIB3 siRNA. Interestingly, the concomitant exposure to TRIB3 siRNA and

perifosine/sorafenib completely inhibited ROS generation by L-540 cells (Supplementary Figure 3d). These results indicate that cell death induced by perifosine/sorafenib requires TRIB3 upregulation and ROS production, resulting in the activation of a necroptotic cell death pathway.

#### Combining perifosine with sorafenib enhances *in vivo* antitumor effects

The *in vivo* antitumor activity of the combined perifosine/sorafenib treatment was investigated in both systemic and localized models of human tumor xenografts in nonobese diabetic/severe combined immunodeficient mice. A model of disseminated disease using intravenously-injected HD-MyZ cells was used to analyze the treatment's effects on both toxicity and survival. No significant changes in weight or other signs of potential toxicity were observed during the treatment with perifosine, sorafenib or the combined treatment (Figure 6a). The median overall survival of mice that were treated with perifosine or sorafenib used as single agents failed to show any statistically significant difference (Figure 6b), whereas the perifosine/sorafenib combination resulted in a significant increase in the median survival compared with untreated controls (45 vs 81 days,  $P < 0.0001$ ) and mice receiving either perifosine (49 vs 81,  $P < 0.03$ ) or sorafenib alone (54 vs 81,  $P < 0.007$ ) (Figure 6b). In addition, 15% of the mice receiving the combined treatment were

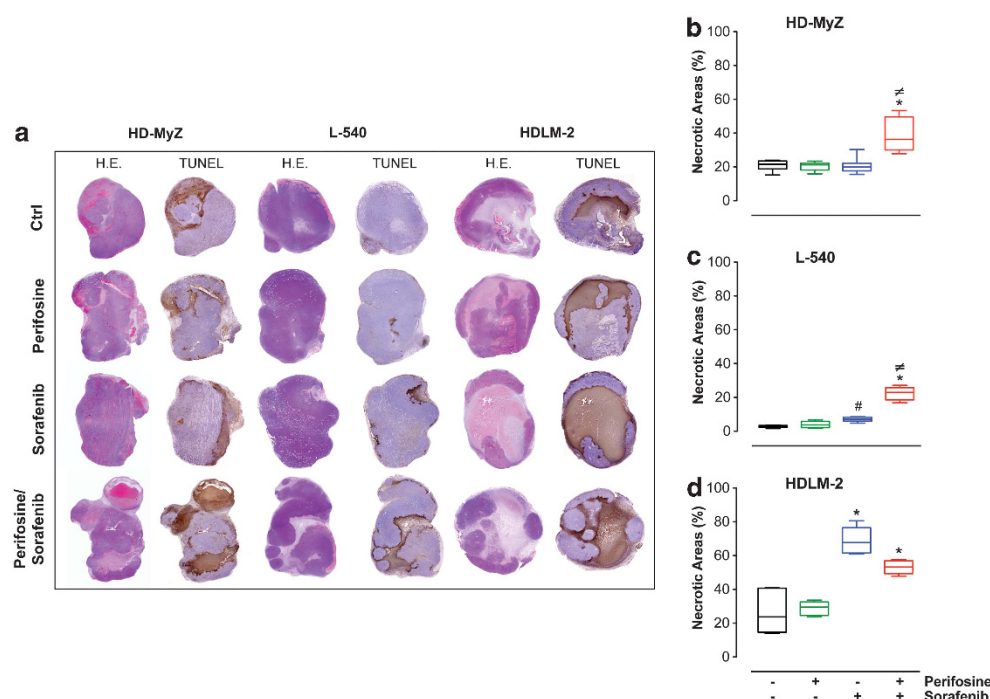


**Figure 7.** Quantification of tumor necrosis within entire tumor sections. NOD/SCID mice bearing subcutaneous tumor nodules 100 mg in weight were randomly assigned to receive a 5-day treatment with perifosine (30 mg/kg/day, PO) and/or sorafenib (90 mg/kg/day, IP) or vehicle control. **(a)** Representative histological images of entire tumors sections from mice that received the different treatments are shown. Tumor tissue morphology was detected by hematoxylin and eosin staining. Tumor necrotic areas were detected by TUNEL staining, and were revealed as brown areas using 3,3'-diaminobenzidine for light microscopy analysis. Objective lens, original magnification: 0.08 NA dry objective,  $\times 2$ . **(b–d)** Digitally acquired TUNEL-stained sections were analyzed using ImageJ for the quantification of tumor necrosis percentage. At least three sections from different animals were analyzed per treatment group. The boxes extend from the 25th to the 75th percentile, the lines indicate the median values, and the whiskers indicate the range of values. \* $P < 0.0001$  and # $P < 0.01$  in comparison with controls.  $^{\#}P < 0.0001$  in comparison with single treatments.

alive and healthy at the end of the 200-day observation period, which strongly supports the efficacy of the combined treatment (Figure 6b).

Two models of localized disease using subcutaneous-injected L-540 and HDLM-2 cell lines were used to analyze the antitumor activity of perifosine in combination with sorafenib. *In vivo* treatment with either perifosine or sorafenib failed to affect the growth of L-540 nodules compared with vehicle-treated controls ( $2.3 \pm 0.3$  vs  $2.8 \pm 0.2$  vs  $2.6 \pm 0.1$  g,  $P > 0.5$ , respectively) (Figure 6c). Despite the lack of activity of the single-agent treatments, the perifosine/sorafenib combination significantly reduced tumor growth as compared with the controls ( $1.5 \pm 0.2$  vs  $2.6 \pm 0.1$  g,  $P < 0.0001$ ), the use of perifosine alone ( $1.5 \pm 0.2$  vs  $2.3 \pm 0.3$  g,  $P < 0.0001$ ) and the use of sorafenib alone ( $1.5 \pm 0.2$  vs  $2.8 \pm 0.2$  g,  $P < 0.0001$ ) with tumor growth inhibition values of 42, 35 and 46%, respectively (Figure 6c). In contrast, the *in vivo* growth of HDLM-2 tumor nodules was not significantly affected by perifosine or sorafenib, either used as single agents or as a combined treatment (Figure 6d).

The extent of areas of tumor necrosis and apoptosis correlates with the *in vivo* antitumor efficacy of the perifosine/sorafenib combination. To elucidate the *in vivo* mechanism(s) of perifosine/sorafenib-induced antilymphoma activity, an accurate quantification of tumor cell death was carried out by evaluating areas of tumor necrosis (by both hematoxylin and eosin staining and TUNEL), as well as the apoptosis of single tumor cells (TUNEL staining). Areas of tumor necrosis, as evaluated in hematoxylin and eosin-stained slides and by the quantitation of diffuse TUNEL staining (Figure 7a), were significantly larger in both HD-MyZ and L-540 nodules following combined perifosine/sorafenib treatment than in controls and single-agent treatments (Figure 7a). The

combined treatment of HD-MyZ tumor nodules induced twofold more tumor necrosis than did single-agent treatments ( $39 \pm 10\%$  vs  $20 \pm 3\%$  vs  $21 \pm 4\%$ ,  $P < 0.0001$ ), and eightfold more tumor necrosis was observed under the same conditions in L-540 nodules than with single-agent treatments ( $22 \pm 4\%$  vs  $4 \pm 2\%$  vs  $7 \pm 1\%$ ,  $P < 0.0001$ ) (Figures 7b and c). Interestingly, in HDLM-2 tumors that were not responsive to the combined treatment, a highly significant increase in necrotic areas was detected in sorafenib-treated mice in comparison with controls (Figure 7d), but the combined treatment failed to promote any additional effects. Computer-aided analysis of TUNEL-stained tumor sections indicated a significant increase in the percentage of apoptotic (TUNEL<sup>+</sup>) tumor cells in mice bearing HD-MyZ and L-540 tumors that were treated with the perifosine/sorafenib combination compared with controls and the use of single treatments (Supplementary Figure 4a). The combined treatment increased the percentage of TUNEL<sup>+</sup> cells in HD-MyZ and L-540 nodules by 2.3- and 2-fold, respectively (Supplementary Figure 4b and c), whereas no effect could be detected on HDLM-2 nodules (Supplementary Figure 4d). Taken together, these results suggest that the *in vivo* antitumor efficacy of the perifosine/sorafenib treatment is associated with the promotion of neoplastic cell death, as identified by the apoptosis of single tumor cells and areas of tumor necrosis.

## DISCUSSION

The cytoprotective role of MEK/ERK1/2 and Akt signaling has focused attention on the combined use of MEK and Akt inhibitors to enhance the antitumor activity of single agents.<sup>36</sup> Indeed, simultaneous targeting of these signaling pathways potentially

induces cell death in transformed cells,<sup>37</sup> suggesting that concomitant inhibition of the MEK/ERK1/2 pathway (for example, by sorafenib) and the Akt pathway (for example, by perifosine) may be an effective treatment option for a variety of diseases characterized by activation of the MAPK and Akt pathways.<sup>10</sup>

We report herein that perifosine combined with sorafenib triggered a variety of antitumor effects both *in vitro* and *in vivo*, including caspase-independent necroptosis and mitochondrial injury, as well as a decreased S-phase fraction and cell viability, and tumor growth inhibition *in vivo*. These events required the constitutive activation of Akt and MEK/ERK1/2 pathways, and were linked to gene expression changes that led to interference with cell signaling pathways, including the inhibition of Akt, MEK/ERK1/2 and Mcl-1 phosphorylation.<sup>19,38</sup> Although individual cell lines showed different levels of Akt and MEK/ERK1/2 activation, data supporting a genetic basis for these differences are not available.

The endogenous inhibitor of Akt, TRIB3, is known to be induced by endoplasmic reticulum stress-induced cell death<sup>39</sup> and was identified as the main mediator of perifosine/sorafenib antitumor activity both *in vitro* and *in vivo*.<sup>19,40</sup> In fact, TRIB3 was potently upregulated by perifosine/sorafenib treatment, whereas its depletion by siRNA significantly reduced perifosine/sorafenib-induced cell death, indicating that the activation of this pseudokinase has a major role in the mechanism of action of perifosine/sorafenib. TRIB3 regulates MAPK pathway and at high levels inhibits this pathway.<sup>33</sup> In addition, TRIB3 binds Akt, preventing the phosphorylation and activation of Akt.<sup>32</sup> TRIB3 upregulation has been linked to antitumor effects in other model systems, including hepatocellular carcinoma where cannabinoids-induced upregulation of TRIB3 inhibits Akt and induces autophagy.<sup>41</sup> Thus, we hypothesize that TRIB3 overexpression may mediate the effects of perifosine and sorafenib via the simultaneous disruption of the Akt and MEK/ERK1/2 pathways, leading to pronounced Akt, ERK and Mcl-1 inactivation (Figure 8).

Perifosine and sorafenib used as single agents mediate CD95-dependent or -independent cell death,<sup>42,43</sup> autophagy<sup>44,45</sup> and caspase-dependent<sup>46</sup> or -independent apoptosis.<sup>47</sup> Such functional heterogeneity in sustaining cell death might be due to the use of different cell models. In this study, we demonstrate that perifosine in combination with sorafenib induces ROS-dependent programmed necrotic cell death, necroptosis. As a consequence, necroptosis inhibition by Necrostatin-1 and TRIB3 silencing by siRNA completely prevented perifosine/sorafenib-induced ROS generation, suggesting a link between caspase-independent necroptosis and endoplasmic reticulum stress-induced cell death.<sup>48</sup>

The existence of necroptotic forms of death was corroborated by the discovery of key executioners such as the kinase RIP1<sup>49</sup> or the mitochondrial protein apoptosis-inducing factor.<sup>50</sup> Upon exposure of L-540 cells to perifosine and sorafenib, extensive translocation of apoptosis-inducing factor to the cytosol and marked cell death occurs. Furthermore, the induction of apoptosis or the activation of cleaved caspase in response to perifosine and sorafenib used as single agents or in combination was not observed in the HD-MyZ cell line, suggesting that in this cell line, the mechanism of action of perifosine and sorafenib is predominantly cytostatic and not cytotoxic, and may be mediated by G2 phase arrest. Additionally, Mcl-1 downregulation likely has an important functional role in the synergistic induction of cHL cell death via the simultaneous interruption of the MEK/ERK1/2 and Akt pathways using the combined perifosine/sorafenib treatment.

Modulation of the Akt and MAPK signaling pathways and their involvement in triggering apoptosis induced by perifosine and sorafenib used as single agents has been studied in a variety of cancer cell types.<sup>18,47,51,52</sup> We report that the perifosine/sorafenib combination significantly affected the MAPK and Akt signaling pathways to a greater extent than did treatment with single agents in two out of three cell lines examined, and the potency of

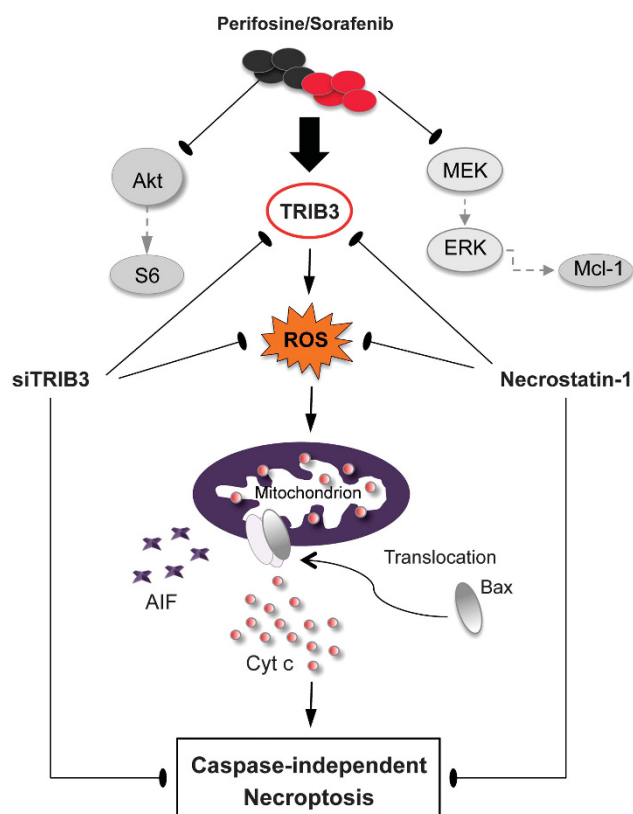


**Figure 8.** Proposed model of perifosine/sorafenib mechanism of action. The combined perifosine/sorafenib treatment triggers necroptotic cell death that is mediated by the production of ROS. Upregulation of TRIB3 enhanced perifosine/sorafenib pathway inhibition and ROS generation, resulting in Bax conformational change and activation, mitochondrial outer membrane permeabilization, release of cytochrome c, and AIF, ultimately leading to caspase-independent necroptosis.

this effect was associated with cHL cell sensitivity to perifosine/sorafenib-anti-lymphoma activity. Interestingly, constitutive phospho-Akt levels were lower in the less sensitive HDLM-2 cells than in the sensitive HD-MyZ and L-540 cells, suggesting that Akt activation is critical in perifosine/sorafenib-mediated cell death.<sup>53</sup>

Although perifosine and sorafenib showed limited efficacy *in vivo* when used as single agents, the combination resulted in a significantly enhanced activity both in HD-MyZ- and L-540-, but not HDLM-2-bearing mice, resulting in an overall good correlation between *in vitro* and *in vivo* data.

Although sharing many key similarities with primary neoplastic cells microdissected from lymph node biopsies, cHL cell lines display major differences in their genome-wide expression program, including a much higher proliferation signature and a much lower interaction with the microenvironment,<sup>54</sup> suggesting caution when extrapolating to patients the results obtained in cHL cell lines, and indicating that new preclinical models are needed to validate more accurately the therapeutic potential of biologically based translational treatment strategies for cHL patients.

Several bona fide HL cell lines have been established,<sup>25</sup> and their *in vitro* and *in vivo* use in immunodeficient mice has provided substantial insights into the pathogenesis of cHL as well as models for preclinical testing of novel agents. However, several lines of evidence suggest caution when extrapolating preclinical data to the clinical setting. First, cHL in humans is a peculiar neoplastic disorder, in whom pathological lymph nodes include less than 10% tumor cells surrounded by more than 90% microenvironmental cells. Thus, in no instance cHL cell lines can

ricapitulate neither *in vitro* nor *in vivo* such a disease complexity. Second, despite the close resemblance in immunophenotype, cHL-derived cell lines are not generally accepted as being truly derived from Hodgkin and Reed-Sternberg or lymphocytic and histiocytic cells. Third, two cell lines (HDLM-2 and L-540) used in our study are of T-cell origin, thus reflecting a rare *in vivo* situation, where B-cell cases far outnumber T-cell cases. Additionally, despite being used by many authors as a cHL-derived cell line, HD-MyZ cell line differs strikingly from *in situ* Hodgkin and Reed-Sternberg cells, as it expresses the macrophage-associated CD68 antigen and lacks expression of CD30 and CD15, as well as rearrangement of immunoglobulin or T-cell receptor genes, thus reflecting its histiocytic derivation.

Owing to the limitations of currently available therapies, there is an urgent need for new therapeutic options for relapsed/refractory cHL patients.<sup>55</sup> Drugs used in the present study are either already approved for clinical indications other than cHL or in active clinical development. The preclinical activity that we observed warrants further investigation and represents a strong rationale for phase I/II studies, combining perifosine and sorafenib treatment in cHL patients.

## CONFLICT OF INTEREST

The authors declare no conflict of interest.

## ACKNOWLEDGEMENTS

This work was supported in part by grants from the Ministry of Education, University and Research (Rome, Italy), the Ministry of Health (Ricerca Finalizzata 2008 and 2010 to CC-S), and the Italian Association for Cancer Research (MCO—9998) (AMG and CC-S).

## REFERENCES

- Lowry L, Hoskin P, Linch D. Developments in the management of Hodgkin's lymphoma. *Lancet* 2010; **375**: 786–788.
- Siegel R, DeSantis C, Virgo K, Stein K, Mariotto A, Smith T et al. Cancer treatment and survivorship statistics, 2012. *CA: A Cancer Journal for Clinicians* 2012; **62**: 220–241.
- Crump M. Management of Hodgkin lymphoma in relapse after autologous stem cell transplant. *Hematology Am Soc Hematol Educ Program* 2008; **1**: 326–333.
- Moskowitz AJ, Perales M-A, Kewalramani T, Yahalom J, Castro-Malaspina H, Zhang Z et al. Outcomes for patients who fail high dose chemoradiotherapy and autologous stem cell rescue for relapsed and primary refractory Hodgkin lymphoma. *Br J Haematol* 2009; **146**: 158–163.
- Younes A. Beyond chemotherapy: new agents for targeted treatment of lymphoma. *Nat Rev Clin Oncol* 2011; **8**: 85–96.
- Younes A, Bartlett NL, Leonard JP, Kennedy DA, Lynch CM, Sievers EL et al. Brentuximab vedotin (SGN-35) for relapsed CD30-positive lymphomas. *N Engl J Med* 2010; **363**: 1812–1821.
- Re D, Thomas RK, Behringer K, Diehl V. From Hodgkin disease to Hodgkin lymphoma: biologic insights and therapeutic potential. *Blood* 2005; **105**: 4553–4560.
- Dickinson M, Ritchie D, DeAngelo DJ, Spencer A, Ottmann OG, Fischer T et al. Preliminary evidence of disease response to the pan deacetylase inhibitor panobinostat (LBH589) in refractory Hodgkin Lymphoma. *Br J Haematol* 2009; **147**: 97–101.
- Boll B, Borchmann P, Diehl V. Emerging drugs for Hodgkin's lymphoma. *Expert Opin Emerg Drugs* 2010; **15**: 585–595.
- De J, Brown RE. Tissue-microarray based immunohistochemical analysis of survival pathways in nodular sclerosing classical Hodgkin lymphoma as compared with Non-Hodgkin's lymphoma. *Int J Clin Exp Med* 2010; **3**: 55–68.
- Younes A. Novel treatment strategies for patients with relapsed classical Hodgkin lymphoma. *Hematology Am Soc Hematol Educ Program* 2009; 507–519.
- Zheng B, Fiumara P, Li YV, Georgakis G, Snell V, Younes M et al. MEK/ERK pathway is aberrantly active in Hodgkin disease: a signaling pathway shared by CD30, CD40, and RANK that regulates cell proliferation and survival. *Blood* 2003; **102**: 1019–1027.
- Richardson PG, Wolf J, Jakubowski A, Zonder J, Lonial S, Irwin D et al. Perifosine plus bortezomib and dexamethasone in patients with relapsed/refractory multiple myeloma previously treated with bortezomib: results of a multicenter phase I/II trial. *J Clin Oncol* 2011; **29**: 4243–4249.
- Mitsiades CS, Hideshima T, Chauhan D, McMillin DW, Klippel S, Laubach JP et al. Emerging treatments for multiple myeloma: beyond immunomodulatory drugs and bortezomib. *Semin Hematol* 2009; **46**: 166–175.
- Pinton G, Manente AG, Angeli G, Mutti L, Moro L. Perifosine as a potential novel anti-cancer agent inhibits EGFR/MET-AKT axis in malignant pleural mesothelioma. *PLoS One* 2012; **7**: e36856.
- Dasmahapatra GP, Didolkar P, Alley MC, Ghosh S, Sausville EA, Roy KK. *In vitro* combination treatment with perifosine and UCN-01 demonstrates synergism against prostate (PC-3) and lung (A549) epithelial adenocarcinoma cell lines. *Clin Cancer Res* 2004; **10**: 5242–5252.
- Nyakern M, Cappellini A, Mantovani I, Martelli AM. Synergistic induction of apoptosis in human leukemia T cells by the Akt inhibitor perifosine and etoposide through activation of intrinsic and Fas-mediated extrinsic cell death pathways. *Mol Cancer Ther* 2006; **5**: 1559–1570.
- Hideshima T, Catley L, Yasui H, Ishitsuka K, Raje N, Mitsiades C et al. Perifosine, an oral bioactive novel alkylphospholipid, inhibits Akt and induces *in vitro* and *in vivo* cytotoxicity in human multiple myeloma cells. *Blood* 2006; **107**: 4053–4062.
- Rahmani M, Reese E, Dai Y, Bauer C, Payne SG, Dent P et al. Coadministration of histone deacetylase inhibitors and perifosine synergistically induces apoptosis in human leukemia cells through Akt and ERK1/2 inactivation and the generation of ceramide and reactive oxygen species. *Cancer Res* 2005; **65**: 2422–2432.
- Wilhelm SM, Adnane L, Newell P, Villanueva A, Llovet JM, Lynch M. Preclinical overview of sorafenib, a multitargeted inhibitor that targets both Raf and VEGF and PDGF receptor tyrosine kinase signaling. *Mol Cancer Ther* 2008; **7**: 3129–3140.
- Guidetti A, Carlo-Stella C, Locatelli SL, Malorni W, Pierdominici M, Barbati C et al. Phase II study of sorafenib in patients with relapsed or refractory lymphoma. *Br J Haematol* 2012; **158**: 108–119.
- Diehl V, Kirchner HH, Schaadt M, Fonatsch C, Stein H, Gerdes J et al. Hodgkin's disease: establishment and characterization of four *in vitro* cell lines. *J Cancer Res Clin Oncol* 1981; **101**: 111–124.
- Drexler HG, Gaedicke G, Lok MS, Diehl V, Minowada J. Hodgkin's disease derived cell lines HDLM-2 and L-428: comparison of morphology, immunological and isoenzyme profiles. *Leuk Res* 1986; **10**: 487–500.
- Bargou RC, Mapara MY, Zugck C, Daniel PT, Pawlita M, Dohner H et al. Characterization of a novel Hodgkin cell line, HD-MyZ, with myelomonocytic features mimicking Hodgkin's disease in severe combined immunodeficient mice. *J Exp Med* 1993; **177**: 1257–1268.
- Küppers R, Re D. Nature of Reed-Sternberg and L & H cells, and their molecular biology in Hodgkin lymphoma. In: Hoppe RT, Mauch PM, Armitage JO, Diehl V (eds) *Hodgkin Lymphoma*. Lippincott Williams & Wilkins, 2007, pp 74–88.
- Carlo-Stella C, Guidetti A, Di Nicola M, Lavazza C, Cleris L, Sia D et al. IFN-gamma enhances the antimyeloma activity of the fully human anti-human leukocyte antigen-DR monoclonal antibody 1D09C3. *Cancer Res* 2007; **67**: 3269–3275.
- Carlo-Stella C, Di Nicola M, Turco MC, Cleris L, Lavazza C, Longoni P et al. The anti-human leukocyte antigen-DR monoclonal antibody 1D09C3 activates the mitochondrial cell death pathway and exerts a potent antitumor activity in lymphoma-bearing nonobese diabetic/severe combined immunodeficient mice. *Cancer Research* 2006; **66**: 1799–1808.
- Lavazza C, Carlo-Stella C, Giacomini A, Cleris L, Righi M, Sia D et al. Human CD34+ cells engineered to express membrane-bound tumor necrosis factor-related apoptosis-inducing ligand target both tumor cells and tumor vasculature. *Blood* 2010; **115**: 2231–2240.
- Chou TC, Talalay P. Quantitative analysis of dose-effect relationships: the combined effects of multiple drugs or enzyme inhibitors. *Adv Enzyme Regul* 1984; **22**: 27–55.
- Zhang J, Yang PL, Gray NS. Targeting cancer with small molecule kinase inhibitors. *Nat Rev Cancer* 2009; **9**: 28–39.
- Kim YS, Jin HO, Seo SK, Woo SH, Choe TB, An S et al. Sorafenib induces apoptotic cell death in human non-small cell lung cancer cells by down-regulating mammalian target of rapamycin (mTOR)-dependent survivin expression. *Biochem Pharmacol* 2011; **82**: 216–226.
- Du K, Herzig S, Kulkarni RN, Montminy M. TRB3: a tribbles homolog that inhibits Akt/PKB activation by insulin in liver. *Science* 2003; **300**: 1574–1577.
- Kiss-Toth E, Bagstaff SM, Sung HY, Jozsa V, Dempsey C, Caunt JC et al. Human tribbles, a protein family controlling mitogen-activated protein kinase cascades. *J Biol Chem* 2004; **279**: 42703–42708.
- Degterev A, Hitomi J, Germesheid M, Ch'en IL, Korkina O, Teng X et al. Identification of RIP1 kinase as a specific cellular target of necrostatins. *Nature Chemical Biology* 2008; **4**: 313–321.
- Cho YS, Challa S, Moquin D, Genga R, Ray TD, Guildford M et al. Phosphorylation-driven assembly of the RIP1-RIP3 complex regulates programmed necrosis and virus-induced inflammation. *Cell* 2009; **137**: 1112–1123.
- Teachey DT, Grupp SA, Brown VI. Mammalian target of rapamycin inhibitors and their potential role in therapy in leukaemia and other haematological malignancies. *Br J Haematol* 2009; **145**: 569–580.

- 37 Stommel JM, Kimmelman AC, Ying H, Nabioullin R, Ponugoti AH, Wiedemeyer R *et al*. Coactivation of receptor tyrosine kinases affects the response of tumor cells to targeted therapies. *Science* 2007; **318**: 287–290.
- 38 Hoeflich KP, O'Brien C, Boyd Z, Cavet G, Guerrero S, Jung K *et al*. *In vivo* antitumor activity of MEK and phosphatidylinositol 3-kinase inhibitors in basal-like breast cancer models. *Clin Cancer Res* 2009; **15**: 4649–4664.
- 39 Ohoka N, Yoshii S, Hattori T, Onozaki K, Hayashi H. TRB3, a novel ER stress-inducible gene, is induced via ATF4-CHOP pathway and is involved in cell death. *EMBO J* 2005; **24**: 1243–1255.
- 40 Rahmani M, Davis EM, Crabtree TR, Habibi JR, Nguyen TK, Dent P *et al*. The kinase inhibitor sorafenib induces cell death through a process involving induction of endoplasmic reticulum stress. *Mol Cell Biol* 2007; **27**: 5499–5513.
- 41 Vara D, Salazar M, Olea-Herrero N, Guzman M, Velasco G, Diaz-Laviada I. Anti-tumoral action of cannabinoids on hepatocellular carcinoma: role of AMPK-dependent activation of autophagy. *Cell Death Differ* 2011; **18**: 1099–1111.
- 42 Gills JJ, Dennis PA. Perifosine: update on a novel Akt inhibitor. *Curr Oncol Rep* 2009; **11**: 102–110.
- 43 Walker T, Mitchell C, Park MA, Yacoub A, Graf M, Rahmani M *et al*. Sorafenib and vorinostat kill colon cancer cells by CD95-dependent and -independent mechanisms. *Mol Pharmacol* 2009; **76**: 342–355.
- 44 Fu L, Kim YA, Wang X, Wu X, Yue P, Lonial S *et al*. Perifosine inhibits mammalian target of rapamycin signaling through facilitating degradation of major components in the mTOR axis and induces autophagy. *Cancer Res* 2009; **69**: 8967–8976.
- 45 Bareford MD, Park MA, Yacoub A, Hamed HA, Tang Y, Cruickshanks N *et al*. Sorafenib enhances pemetrexed cytotoxicity through an autophagy-dependent mechanism in cancer cells. *Cancer Res* 2011; **71**: 4955–4967.
- 46 Chiarini F, Del Sole M, Mongiorgi S, Gaboardi GC, Cappellini A, Mantovani I *et al*. The novel Akt inhibitor, perifosine, induces caspase-dependent apoptosis and downregulates P-glycoprotein expression in multidrug-resistant human T-acute leukemia cells by a JNK-dependent mechanism. *Leukemia* 2008; **22**: 1106–1116.
- 47 Floryk D, Thompson TC. Perifosine induces differentiation and cell death in prostate cancer cells. *Cancer Letters* 2008; **266**: 216–226.
- 48 Dengler MA, Staiger AM, Gutekunst M, Hofmann U, Doszczak M, Scheurich P *et al*. Oncogenic stress induced by acute hyper-activation of Bcr-Abl leads to cell death upon induction of excessive aerobic glycolysis. *PLoS One* 2011; **6**: e25139.
- 49 Christofferson DE, Yuan J. Necroptosis as an alternative form of programmed cell death. *Curr Opin Cell Biol* 2010; **22**: 263–268.
- 50 Baritaud M, Cabon L, Delavallee L, Galan-Malo P, Gilles ME, Brunelle-Navas MN *et al*. AIF-mediated caspase-independent necroptosis requires ATM and DNA-PK-induced histone H2AX Ser139 phosphorylation. *Cell Death Dis* 2012; **3**: e390.
- 51 Vink SR, van Blitterswijk WJ, Schellens JH, Verheij M. Rationale and clinical application of alkylphospholipid analogues in combination with radiotherapy. *Cancer Treat Rev* 2007; **33**: 191–202.
- 52 Nguyen TK, Jordan N, Friedberg J, Fisher RI, Dent P, Grant S. Inhibition of MEK/ERK1/2 sensitizes lymphoma cells to sorafenib-induced apoptosis. *Leuk Res* 2010; **34**: 379–386.
- 53 Hennessy BT, Lu Y, Poradosu E, Yu Q, Yu S, Hall H *et al*. Pharmacodynamic markers of perifosine efficacy. *Clin Cancer Res* 2007; **13**: 7421–7431.
- 54 Tiaci E, Doring C, Brune V, van Noesel CJ, Klapper W, Mechttersheimer G *et al*. Analyzing primary Hodgkin and Reed-Sternberg cells to capture the molecular and cellular pathogenesis of classical Hodgkin lymphoma. *Blood* 2012; **120**: 4609–4620.
- 55 Cramer P, Hallek M. Hematological cancer in 2011: new therapeutic targets and treatment strategies. *Nat Rev Clin Oncol* 2012; **9**: 72–74.

Supplementary Information accompanies the paper on the Leukemia website (<http://www.nature.com/leu>)